An aeroacoustics-based approach for wind turbine blade damage detection

Zhang, Y.; Avallone, F.; Watson, S.J.

DOI
10.1088/1742-6596/2265/2/022088

Publication date
2022

Document Version
Final published version

Published in
Journal of Physics: Conference Series

An aeroacoustics-based approach for wind turbine blade damage detection

An aeroacoustics-based approach for wind turbine blade damage detection

Yanan Zhang*; Francesco Avallone; Simon Watson

Wind Energy Section, Faculty of Aerospace Engineering, Delft University of Technology, Delft, 2629HS, The Netherlands

*E-mail: Yanan.Zhang@tudelft.nl

Abstract. In this work, aimed at the development of an aeroacoustics-based wind turbine blade damage detection approach, the noise scattered from two airfoils with damage at the trailing edge or at the leading edge is investigated. Four trailing edge cracks (with width of 0.2, 0.5, 1.0 and 2.0 mm) and four leading edge erosion configurations (consisting of gouges and delamination) are investigated for a NACA 0018 and a DU96 W180 airfoil. Experiments are carried out under clean and turbulent inflow conditions. Acoustic measurements are performed in an anechoic wind tunnel with a microphone array. The trailing edge crack causes a tonal peak at trailing-edge-thickness-based Strouhal number approximately equal to $St_h \sim 0.1$ under clean and low turbulence intensity inflow conditions (e.g. ~4% in this study). For a higher turbulence intensity (e.g., ~7%), the tonal peaks are not detectable. For the leading edge erosion case, under clean inflow conditions and minor damage levels, the amplitudes of the harmonics in the trailing edge noise spectra increase compared with the baseline. For moderate damage levels, the harmonics on the suction side shift to higher frequencies with lower amplitudes. For the highest damage levels, only broadband characteristics are present, where low-frequency contributions increase and high-frequency contributions decrease as the damage level increases. When introducing turbulent inflow, the leading edge impingement noise level decreases at medium-high frequency (above 1000 Hz) with increasing levels of erosion.

1 Introduction

With increasing energy generated by wind turbines, condition monitoring and damage detection are important to ensure operational safety and plant availability. Due to harsh operating environments and material aging, wind turbine blades are subject to various types of damage and failures. Moreover, blades have a greater probability of damage than other components, for example, generators or gearboxes [1].

To date, the most common way to avoid severe blade failures is to perform testing in the laboratory before mounting the blades [2]. However, it is difficult to extend laboratory testing approaches to the real-time condition monitoring of blades for practical reasons. For an operating wind turbine, measurements of vibration [3], strain [4] or acoustic emission (AE) [5] of the blade are commonly used for damage detection. However, only sensors close to the damage locations can provide accurate information for the damage detection. Moreover, the sensors are required to be mounted on or inside the blades. This makes the installation of such sensors challenging once the blades have already been installed and are operational. A few attempts have been carried out to provide non-contact and remote solutions for damage detection, for example, by using infrared thermographic cameras [6], laser scanners

[7] or microphones [8]. Those techniques improve the flexibility of blade damage detection for the purpose of real-time applications to some extent.

When damage is present in a wind turbine blade, changes in surface roughness or airfoil shape can affect aerodynamic-generated noise. Compared with a clean airfoil, the damage on the surface, for example, caused by leading edge erosion or coating shedding, affects the boundary layer transition location, which results in a variation of the turbulent boundary layer integral quantities at the trailing edge; this causes a change in the noise scattered from the trailing edge [9]. Under turbulent inflow conditions, the eroded leading edge might lead to a larger stagnation region [10] where the chord-wise velocity goes to zero and the normal direction component increases. The convection speed and direction of turbulent fluctuations are changed and the magnitudes of the turbulent velocities incident on the airfoil are reduced [10]. This affects the spectra of leading-edge impingement noise. Certain failures of the trailing edge adhesive joint such as cracks result in a thicker trailing edge; when the thickness of the trailing edge is larger than 0.3 times the boundary layer displacement thickness at the trailing edge, then vortex shedding occurs resulting in tonal noise in the far-field spectrum [11]. These noise spectral features can be measured by microphones located remotely, thus providing a potential non-contact damage detection solution for blade health condition monitoring. A few studies [12] have tried to use such aeroacoustic information from a data-driven perspective for damage detection by means of measuring in-field wind turbine noise.

In this study, we focus on blade damage detection involving leading edge erosion and trailing edge cracks based on airfoil aeroacoustic noise. A microphone array is used which allows different sound sources scattered from the airfoil to be measured and analyzed. In a real-world application, in addition to causing impingement noise, the presence of turbulent inflow will also alter noise spectral features. In order to investigate the effects of the turbulent inflow on damage detection, the experiments are carried out under two turbulent conditions (with turbulence intensity of ~4% and ~7%).

2 Experimental setup

2.1 Facilities and test models

The experiments were carried out in the anechoic vertical open-jet tunnel (A-tunnel) of Delft University of Technology [13]. The rectangular test section of the wind tunnel is 40 cm × 70 cm, allowing experiments up to 45 m/s free stream velocity under 0.1% turbulence intensity. The uniformity of the mean flow velocity within the entire test section is below 0.5 % with respect to the center velocity of the outlet. To simulate different turbulent inflow conditions, two grids (#1 and #2) are designed to generate turbulence intensity levels of ~ 4% and ~ 7% and turbulence integral length scales of 7.9 mm and 10.2 mm, respectively. The turbulence intensity levels are chosen to correspond to the range of conditions seen in the field at an offshore site [14].

Two airfoils, a NACA 0018 and a DU96 W180, with span length, L, of 400 mm and chord length, C, of 200 mm were investigated. The selection of these two types of airfoils is for comparison with previous studies on trailing-edge noise [15] and leading-edge erosion [16]. These two airfoils are modular with changeable trailing edge and leading edge parts, thus allowing the testing of different types and severities of damage. Figure 1 shows the test models.

Four damaged trailing edge parts for the NACA 0018 airfoil are investigated with crack width, W, of 0.2, 0.5, 1.0 and 2.0 mm (with scaling ratios of W/C equal to 0.10%, 0.25%, 0.50% and 1.0%, respectively). This leads to an effective trailing edge thickness, h, of 0.96, 1.26, 1.76 and 2.76 mm, respectively (giving scaling ratios of h/C equal to 0.48%, 0.63%, 0.88% and 1.38%, respectively). Figure 1(a) shows an example for the 0.2 mm width crack.

Leading edge erosion features for the DU96 W180 airfoil are simulated with gouges (1.0 mm diameter and depth) and coating delamination (1.5 mm depth). The gouges (G) are distributed within 10% and 13% of the chord on the suction and pressure surfaces, respectively. For different delamination levels (DL, DL+ and DL++), the delamination area is extended to 2, 4 and 6 mm on the suction side and

2.6, 5.2 and 7.8 mm on pressure side, respectively. The damage sizes are scaled based on eroded blades provided by 3M as reported in [16]. Figure 1(b) shows an example for erosion damage level 4. Details of each configuration are shown in Table 1.

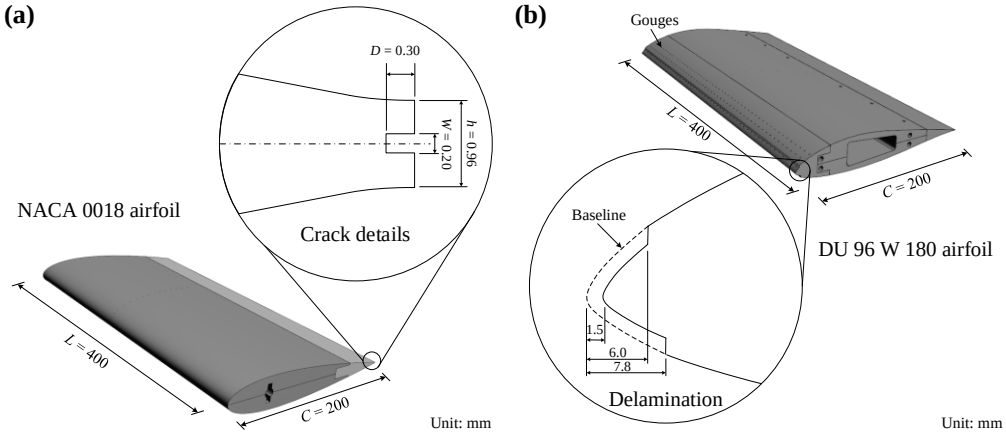

Figure 1. Test models: (a) An example for NACA 0018 airfoil with a 0.2 mm trailing edge crack; (b) an example for DU 96 W180 airfoil with leading edge erosion level 4.

Table 1. Leading edge erosion features for different damage levels.

	Baseline	Simulated erosion			
Damage level	0	1	2	3	4
Features	No damage	25 G	50 G/DL	100 G/DL+	200 G/DL++

The experimental setup is shown in Figure 2. The turbulence generating grid was fixed on the wind tunnel nozzle. The airfoil was mounted at 0.3 m from the wind tunnel nozzle plane between two side plates to ensure a 2-dimensional flow. The angles of attack of two airfoils were set to zero and were calibrated using surface static pressure distributions compared with those from XFOIL. To describe the relative positions for the experimental setup, a Cartesian coordinate system (*o-xyz*) is used taking the geometric center of the trailing edge as the origin at an airfoil angle of attack of 0°.

The experiments both for the trailing edge crack detection and leading edge erosion detection were performed using 30 m/s mean flow velocity and an airfoil angle of attack of 0°. Due to the low Reynolds number test condition ($Re = 4.1\times10^5$, based on airfoil chord length), to ensure a turbulent flow at the trailing edge, the NACA 0018 airfoil was tripped using two tripping devices located at 20% of the chord. The tripping devices were made of grits randomly distributed on tapes. To investigate the effect of the erosion on the flow transition, the DU96 W180 airfoil was not tripped.

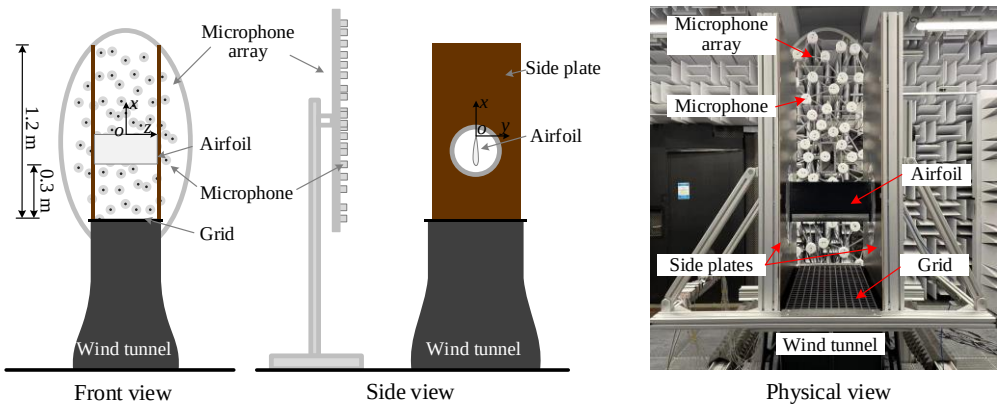

Figure 2. Experimental setup.

2.1.1 Acoustic measurement

A 2-D planar microphone array placed at $y = -1$ m parallel to the airfoil chord line was used for the noise measurement in this study. It contained 64 free-field microphones where the distribution is shown in Figure 3. The sampling frequency of each microphone was 51.2 kHz. For each measurement, the signal was recorded for 20 s. The signal was separated into time blocks of 5120 samples for each Fourier transform thus giving a frequency resolution of 10 Hz. The microphone array allows the analysis of noise scattered from the regions of interest, such as the trailing edge or leading edge, with beamforming and source power integration techniques [17]. In this study, for the trailing edge crack detection, the sound power was integrated within a 0.2 m × 0.2 m region centered at the trailing edge mid-point (black dashed box in Figure 3(a)). For the leading edge erosion detection, there were two integrated regions with a size of 0.2 m × 0.1 m centered at the leading edge and trailing edge mid-points to investigate the noise scattered at both locations respectively (the black and red dashed boxes in Figure 3(b)). The reference microphone is at (0.1, -1.0, 0) m for the trailing edge crack noise detection while for the leading edge erosion noise detection the height is increased to x=0.2 m to avoid the acoustic shadow effect of the wind tunnel nozzle thus improving the quality of the leading edge noise measurements.

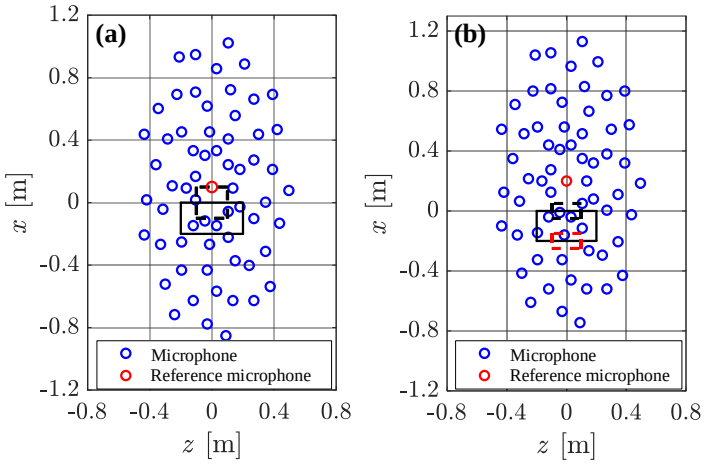

Figure 3. The distribution of microphone array for two experiments: (a) trailing edge crack detection and (b) leading edge erosion detection. The black solid boxes are the projections of the airfoils into the array plane and the black and red dashed boxes represent the sound power integrated regions at the trailing edge and leading edge, respectively.

3 Results and discussion

Sound pressure level (SPL) is chosen as the sound metric of the noise spectra, which is defined as:

$$L_p = 10\lg\left(\frac{p_e^2}{p_{ref}^2}\right) \tag{1}$$

where p_e is the root mean square sound pressure fluctuations and p_{ref} is the reference pressure, which is 20 μPa in air.

3.1 Trailing edge crack detection

3.1.1 Clean flow condition

Figure 4 shows the beamforming maps for the baseline and 2.0 mm crack case in one-third octave band with a central frequency of 1250 Hz. Under the clean flow condition, the noise scattered from the trailing edge is dominant. For the selected band, the SPL for the 2.0 mm crack shows a distinctly higher level than that of the baseline.

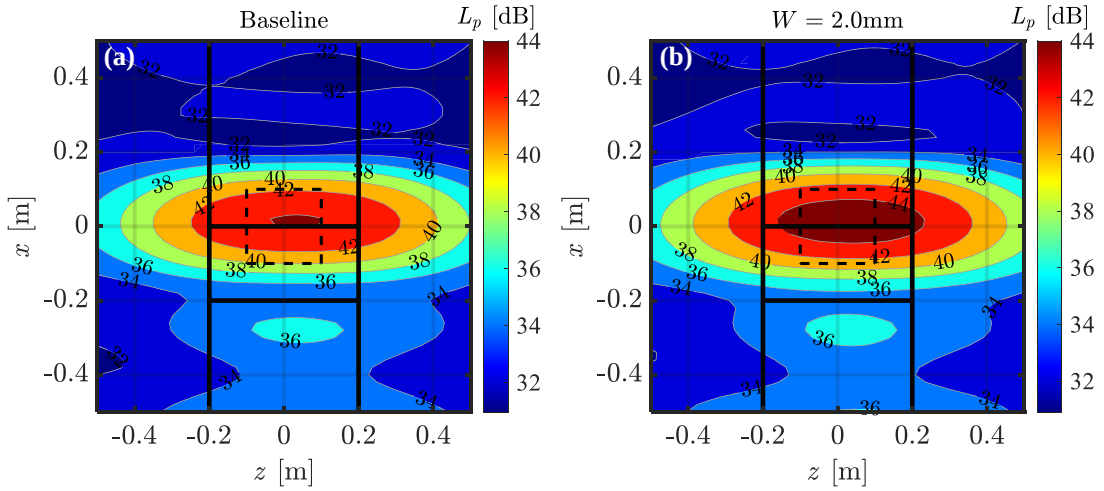

Figure 4. Beamforming maps for one-third octave band at a central frequency of 1250 Hz: (a) baseline and (b) 2.0 mm width crack. The dashed boxes are the integrating regions for the sound power level.

The spectra of L_p for the cases with different crack sizes under clean flow conditions are shown in Figure 5(a). The spectra are integrated from the beamforming results within the region at the trailing edge shown in Figure 3(a) and Figure 4. When looking at the 2.0 mm crack and baseline cases, the noise spectrum for the 2.0 mm crack shows a significant tonal peak at around 1100 Hz but the broadband contributions on both sides of the tone are reduced. The presence of the tone is due to the periodic vortex shedding from a blunt trailing edge and the energy redistribution at this frequency. For the smaller crack cases, this peak is reduced and the location shifts to a higher frequency. Previous studies have suggested that the characteristic frequencies for these peaks can be determined using the trailing-edge-thickness-based Strouhal number, $St_h = fh/\bar{U}$, which is approximately equal to 0.1 [15]. Figure 5(b) shows the spectral differences, $\Delta L_p = L_p - L_{p,Baseline}$, of sound pressure level from the baseline case, in which the frequency is normalized by St_h. Like the spectra of sound pressure level in Figure 5(a), the peak becomes narrower and larger with increasing crack size. Moreover, the location of the peak shifts to a slightly smaller value of St_h. Similar results are reported in [15], which suggested that the location of the tone depends on the ratio of trailing edge thickness to boundary layer displacement thickness.

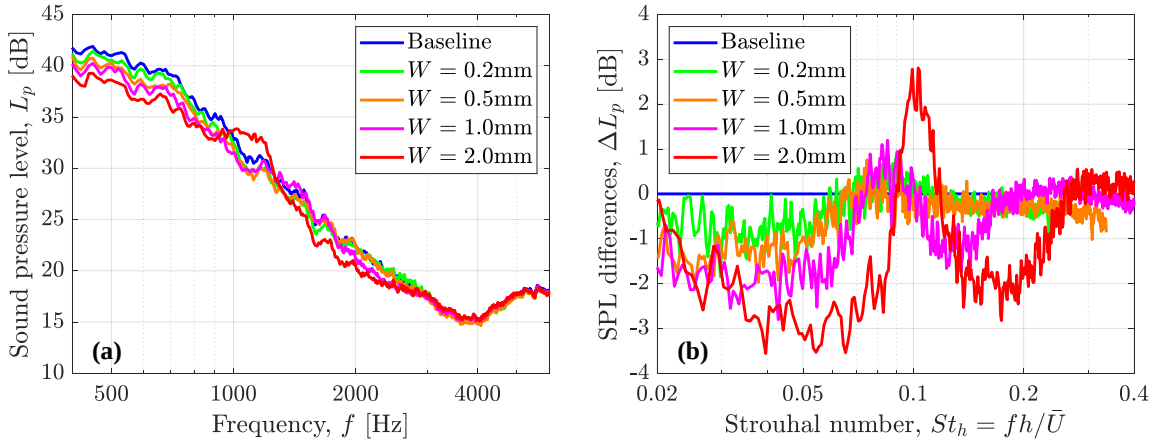

Figure 5. The spectra for different trailing edge crack cases for 30 m/s clean flow conditions at a 0° airfoil angle of attack: (a) sound pressure level against frequency and (b) sound pressure level differences against trailing edge thickness based Strouhal number St_h.

3.1.2 Turbulent inflow conditions

The spectra of ΔL_p under turbulent inflow conditions are shown in Figure 6. When turbulent inflow is introduced, the spectral differences from the baseline are reduced. When at low turbulence intensity (i.e. ~4% with grid #1 mounted), in Figure 6 (a), only for the 1.0 mm and 2.0 mm crack cases, can the peak be distinguished in the spectra. Moreover, the tonal peaks slightly shift to a value of St_h larger than 0.1. However, for the high turbulence intensity case (i.e. ~7% with grid #2 mounted), the damage-induced spectral differences from the baseline are almost indistinguishable.

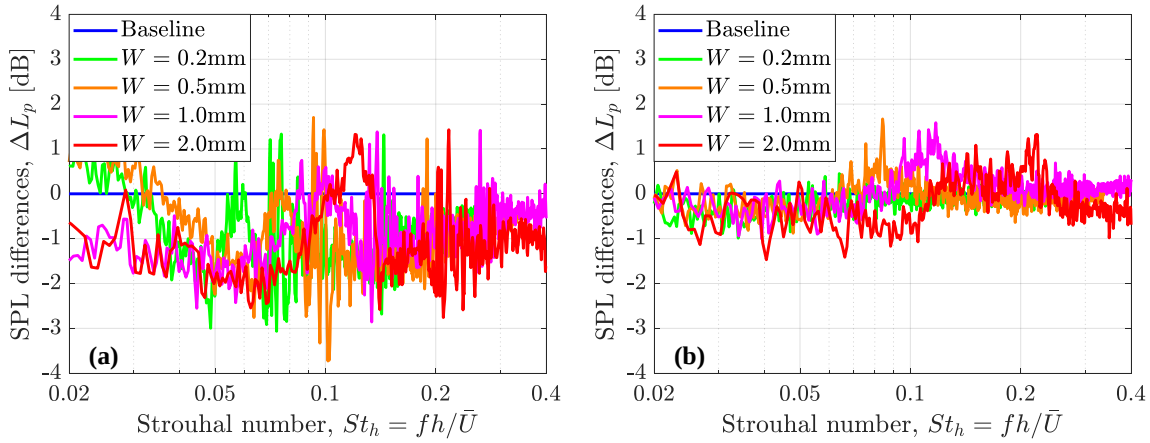

Figure 6. Spectral differences of sound pressure level under turbulent inflow when mean flow velocity is 30 m/s and airfoil angle of attack is 0°: (a) with grid #1 mounted (b) with grid #2 mounted.

3.2 Leading edge erosion detection

3.2.1 Clean flow condition

Figure 7 shows the spectra of L_p for the trailing edge noise both on the suction side and pressure side under clean inflow conditions. For damage level 1, the spectra show laminar instability noise characteristics containing a broadband hump and a set of harmonics. Compared with the healthy airfoil (baseline), the amplitudes of the harmonics are higher. The amplitudes of the dominant tone for damage level 1 and the baseline are 48.36 dB and 41.25 dB, respectively, on the suction side and 55.75 dB and 53.80 dB, respectively, on the pressure side. However, the frequencies of the harmonics in the spectra do not change. This is potentially because the erosion does not change the location where the instabilities originally occur thus leading to similar acoustic feedback lengths.

For damage level 2, on the suction side, laminar boundary layer instability noise is still present. Moreover, the harmonics in this case shift to higher frequencies and their amplitudes are decreased compared with the baseline. On the pressure side, the discrete tones can no longer be seen and the spectrum shows broadband turbulent boundary layer noise characteristics. Similar results were reported in previous studies [18,19], in which the airfoil was tripped on the pressure side. The difference in the spectrum compared with the baseline and damage level 1 case is attributed to suppression for the acoustic feedback on the pressure side without separation bubbles.

For the increased damage levels 3 and 4, the spectra on both sides of the airfoil show only broadband noise. This is because the flow is no longer transitional but turbulent after passing the erosion area thus leading to the absence of laminar boundary layer instability noise. Moreover, with the increase in damage level, the high-frequency contributions decrease but the low-frequency contributions increase. The reason for the variation in far-field noise spectra for damage levels 3 and 4 is that the spectral energy is redistributed to the low frequency region as damage increases.

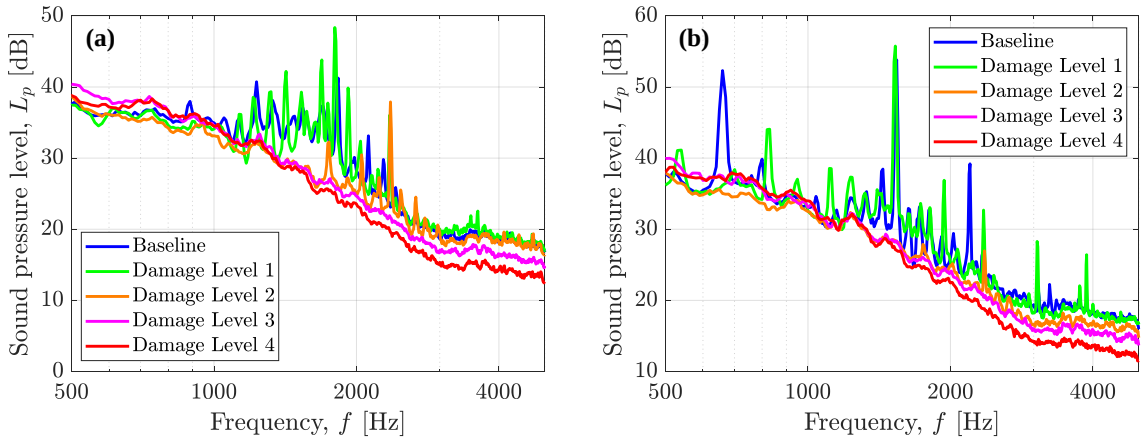

Figure 7. Spectra of sound pressure level at the trailing edge for different erosion levels for 30 m/s clean inflow conditions at a 0° airfoil angle of attack: (a) on the suction side and (b) on the pressure side.

3.2.2 Turbulent inflow conditions

When the airfoil encounters turbulent inflow, it experiences pressure fluctuations at the leading edge. This leads to leading edge impingement noise [10,20–22]. Figure 8 shows the beamforming maps for the baseline and damage level 4 case integrated within a one-third octave band with a central frequency of 1250 Hz. Three sound sources from different locations are present: from the grid, leading edge and trailing edge. Figure 9 shows the spectra of sound pressure levels both at trailing edge and leading edge when mounting grid #1. The frequency range is selected between 500 Hz and 2000 Hz to keep a high signal-to-noise ratio. In Figure 9(b) and (d), the spectra of the noise scattered from the trailing edge for different damage cases and baseline do not show any significant differences. This means it is invalid to use the trailing edge noise for leading edge erosion detection under turbulent inflow conditions.

In Figure 9(a) and (c), the noise scattered from leading edge for different damage levels are shown. With the increase in damage level, the sound pressure level decays above 1000 Hz. For example, within the selected one-third octave band, the peak sound level within the integrated region at the leading edge for damage level 4 case is lower (49.23 dB) than that of the baseline (51.44 dB). This might be attributed to the increasing mean flow stagnation region [10] in front of the leading edge, where the chord-wise velocity goes to zero and the normal direction component increases. In such a stagnation region, the convection of turbulent velocity waves is weakened thus reducing the magnitudes of the turbulent velocities impinging the leading edge; as a consequence, the power of the noise scattered from the leading edge is also reduced.

With higher turbulence intensity (~7% with grid #2 mounted), a similar decay trend of the leading edge noise with the increase in damage level can be seen in Figure 10. However, the differences between the spectra are smaller than the lower turbulence intensity case.

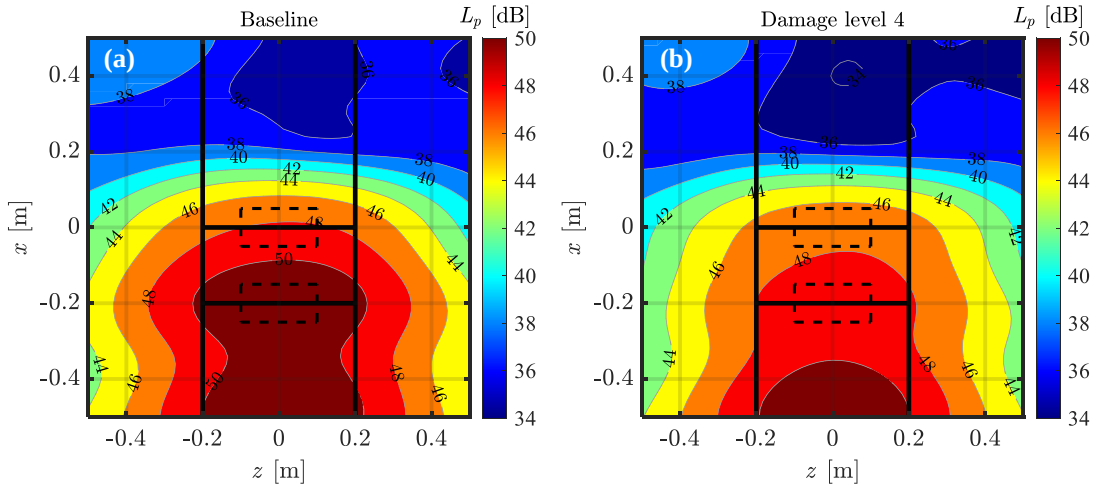

Figure 8. Beamforming maps for a one-third octave band at a central frequency of 1250 Hz for 30 m/s mean flow velocity with grid #1 mounted at a 0° airfoil angle of attack: (a) for baseline and (b) for damage level 4. The dashed boxes are the integrating regions for the sound power level.

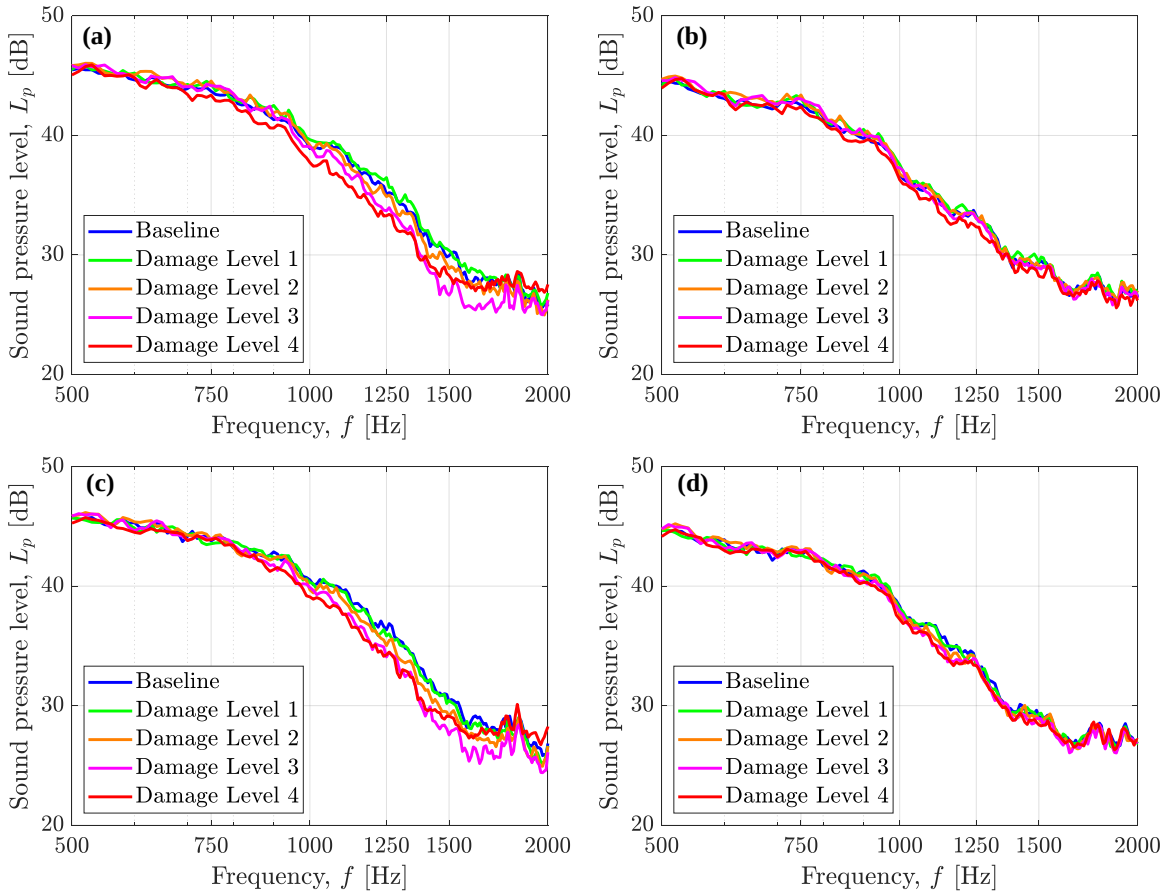

Figure 9. Spectra of sound pressure level for different erosion levels for 30 m/s mean flow velocity with grid #1 mounted at a 0° airfoil angle of attack: (a) at the leading edge on suction side; (b) at the trailing edge on the suction side; (c) at the leading edge on the pressure side; (d) at the trailing edge on the pressure side.

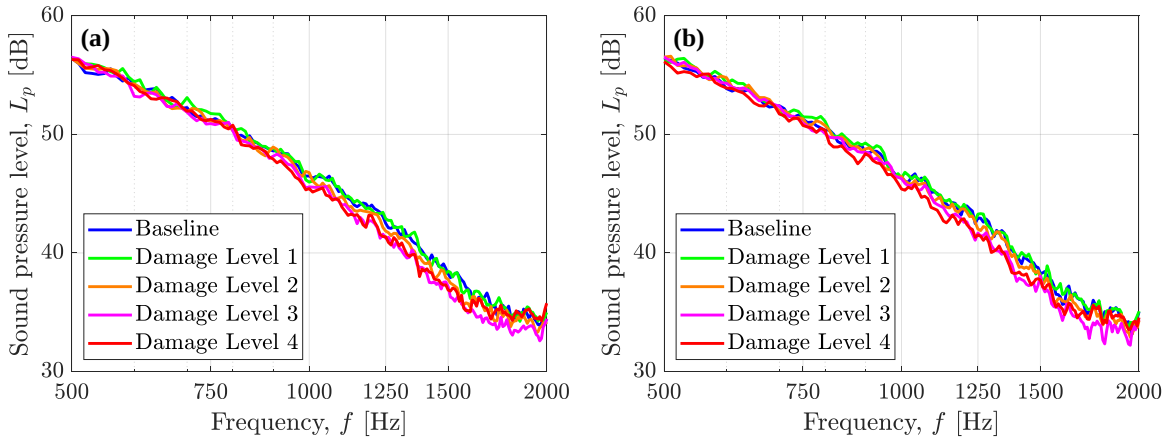

Figure 10. Spectra of sound pressure level at the leading edge for different erosion levels for 30 m/s mean flow velocity with grid #2 mounted at a 0° airfoil angle of attack: (a) on the suction side and (b) on the pressure side.

4 Conclusions and outlook

Simulated blade damage detection based on aerodynamic noise measurements for trailing edge crack and leading edge erosion was investigated. The crack-induced trailing edge bluntness tonal noise peaks were found to occur at a trailing-edge-thickness-based Strouhal number, $St_h \sim 0.1$. It was shown to be possible to detect a trailing edge crack under clean and low turbulence intensity conditions (e.g. ~4% in this study), however, increased turbulence reduced detection sensitivity. This suggests that if such a damage detection approach was used in a real-world situation, longer measurement time averages may be necessary to increase signal-to-noise to make damage induced tonal peaks more visible.

Under clean flow conditions, for a minor erosion level, the amplitudes of the tones caused by laminar boundary layer instability noise increase as the presence of leading edge erosion enhances the transitional process; for higher erosion levels, the tones shift to a higher frequency with lower amplitudes because the flow on the pressure side is turbulent and acoustic feedback loops on the pressure side are suppressed; when the erosion level becomes greater still, the erosion leads to a thicker boundary layer at the trailing edge and the spectral energy is redistributed to lower frequencies. When turbulent inflow is introduced, the spectra from the trailing edge are indistinguishable for all damage levels. However, the sound power level of leading edge impingement noise decreases at medium-high frequency with increasing damage level.

Although the experiments were carried out using 2D airfoils, results are expected to follow a similar trend for a full-scale rotating wind turbine blade as the noise sources are similar. However, when considering realistic applications, a few considerations should be borne in mind. Firstly, since the Reynolds numbers in the field are higher than those in the experiments, the laminar boundary layer instability noise will not be present, thus making it challenging to detect leading edge erosion using trailing edge noise measurements alone. Additionally, the turbulence length scales are usually much larger than the blade chord length; this may lead to a completely different form of leading edge impingement noise and shift the noise spectra. These limitations suggest that to apply an aeroacoustic noise measurement approach to a real wind turbine, a longer monitoring time or other additional measurement techniques would be needed.

Acknowledgement

This work was supported by the China Scholarship Council (CSC) under Grant 201906330095. The authors would like to thank Salil Luesutthiviboon, Dr. Riccardo Zamponi, Dr. Alejandro Rubio Carpio, Dr. Daniele Ragni for their suggestions on experimental design and data processing and Dr. Marios Kotsonis, Kaisheng Peng and Stefan Bernardy for their help with the experimental setup.

References

[1] Ribrant J and Bertling L 2007 Survey of failures in wind power systems with focus on Swedish wind power plants during 1997-2005 *2007 IEEE Power Eng. Soc. Gen. Meet. PES* 1–8
[2] Oliveira M A, Simas Filho E F, Albuquerque M C S, Santos Y T B, da Silva I C and Farias C T T 2020 Ultrasound-based identification of damage in wind turbine blades using novelty detection *Ultrasonics* **108** 106166
[3] Al-Hadad M, McKee K K and Howard I 2019 Vibration characteristic responses due to transient mass loading on wind turbine blades *Eng. Fail. Anal.* **102** 187–202
[4] Schroeder K, Ecke W, Apitz J, Lembke E and Lenschow G 2006 A fibre Bragg grating sensor system monitors operational load in a wind turbine rotor blade *Meas. Sci. Technol.* **17** 1167–72
[5] Bhargava V and Samala R 2019 Acoustic emissions from wind turbine blades *J. Aerosp. Technol. Manag.* **11**
[6] Hwang S, An Y K and Sohn H 2019 Continuous-wave line laser thermography for monitoring of rotating wind turbine blades *Struct. Heal. Monit.* **18** 1010–21
[7] Park B, Sohn H, Malinowski P and Ostachowicz W 2017 Delamination localization in wind turbine blades based on adaptive time-of-flight analysis of noncontact laser ultrasonic signals *Nondestruct. Test. Eval.* **32** 1–20
[8] Solimine J, Niezrecki C and Inalpolat M 2020 An experimental investigation into passive acoustic damage detection for structural health monitoring of wind turbine blades *Struct. Heal. Monit.* **19** 1711–25
[9] Ye Q, Avallone F, Ragni D, Choudhari M and Casalino D 2021 Effect of Surface Roughness Geometry on Boundary-Layer Transition and Far-Field Noise *AIAA J.* 1–13
[10] Kim D, Lee G S and Cheong C 2015 Inflow broadband noise from an isolated symmetric airfoil interacting with incident turbulence *J. Fluids Struct.* **55** 428–50
[11] Oerlemans S 2011 Wind turbine noise : primary noise sources 1–57
[12] Chen B, Yu S, Yu Y and Zhou Y 2020 Acoustical damage detection of wind turbine blade using the improved incremental support vector data description *Renew. Energy* **156** 548–57
[13] Merino-Martínez R, Rubio Carpio A, Lima Pereira L T, van Herk S, Avallone F, Ragni D and Kotsonis M 2020 Aeroacoustic design and characterization of the 3D-printed, open-jet, anechoic wind tunnel of Delft University of Technology *Appl. Acoust.* **170**
[14] Hansen K S, Barthelmie R J, Jensen L E and Sommer A 2012 The impact of turbulence intensity and atmospheric stability on power deficits due to wind turbine wakes at Horns Rev wind farm *Wind Energy* **15** 183–96
[15] Brooks T F, Pope D S and Marcolini M A 1989 *Airfoil self-noise and prediction* vol 1218 (National Aeronautics and Space Administration)
[16] Sareen A, Sapre C A and Selig M S 2014 Effects of leading edge erosion on wind turbine blade performance *Wind Energy* **17** 1531–42
[17] Merino-Martínez R, Sijtsma P, Carpio A R, Zamponi R, Luesutthiviboon S, Malgoezar A M N, Snellen M, Schram C and Simons D G 2019 Integration methods for distributed sound sources *Int. J. Aeroacoustics* **18** 444–69
[18] Dovgal A V., Kozlov V V. and Michalke A 1994 Laminar boundary layer separation: Instability and associated phenomena *Prog. Aerosp. Sci.* **30** 61–94
[19] Pröbsting S and Yarusevych S 2015 Laminar separation bubble development on an airfoil emitting tonal noise *J. Fluid Mech.* **780** 167–91
[20] Lee G-S and Cheong C 2021 Frequency-domain prediction of broadband inflow noise radiating from a finite-thickness airfoil *J. Wind Eng. Ind. Aerodyn.* **213** 104618
[21] Buck S, Oerlemans S and Palo S 2016 Experimental characterization of turbulent inflow noise on a full-scale wind turbine *J. Sound Vib.* **385** 219–38
[22] Faria A M, Saab J Y, Rodriguez S and de Mattos Pimenta M 2020 A rapid distortion theory-based airfoil turbulent inflow noise prediction method *J. Brazilian Soc. Mech. Sci. Eng.* **42** 1–9